# Fermi surface of the superconductor $BaIr_2P_2$

T. Förster,[1] B. Bergk,[1,*] O. Ignatchik,[1] M. Bartkowiak,[2] S. Blackburn,[3] M. Côté,[3] G. Seyfarth,[3,4,5] N. Berry,[5] Z. Fisk,[5] I. Sheikin,[4] A. D. Bianchi,[3] and J. Wosnitza[1,6]

[1]*Hochfeld-Magnetlabor Dresden (HLD-EMFL), Helmholtz-Zentrum Dresden-Rossendorf, D-01314 Dresden, Germany*

[2]*Laboratory for Developments and Methods, Paul Scherrer Institute, CH-5232 Villigen, Switzerland*

[3]*Département de Physique and RQMP, Université de Montréal, Montréal H3C 3J7, Canada*

[4]*Laboratoire National des Champs Magnétiques Intenses (LNCMI-EMFL), CNRS, UJF, F-38042 Grenoble, France*

[5]*Department of Physics and Astronomy, University of California Irvine, Irvine, California 92697, USA*

[6]*Institut für Festkörperphysik, TU Dresden, D-01062 Dresden, Germany*

(Received 28 August 2015; published 20 October 2015)

We report on de Haas–van Alphen (dHvA) and band-structure studies of the iridium-pnictide superconductor $BaIr_2P_2$ ($T_c = 2.1$ K). The observed dHvA frequencies can be well understood by our band-structure calculations with two bands crossing the Fermi energy leading to a strongly corrugated Fermi-surface cylinder around the X point and a highly evolved, multiconnected Fermi surface extending over the whole Brillouin zone. The experimental effective masses are found to be considerably larger than the calculated band masses suggesting strong many-body interactions. Nevertheless, $T_c$ remains only moderate in $BaIr_2P_2$ contrary to isostructural iron pnictides which probably is related to the largely different Fermi-surface topologies in these materials.

DOI: 10.1103/PhysRevB.92.134518 PACS number(s): 71.18.+y, 74.25.Jb, 74.70.Xa

Shortly after the discovery of superconductivity in iron-pnictide compounds [1] the question arose whether this material combination is decisive for the realization of high superconducting transition temperatures. One route—of the many possible ones—to investigate this is the substitution of Fe by other transition-metal elements. Predominantly, this was done for the ternary 122 material class, that forms in the tetragonal $ThCr_2Si_2$ structure, for which superconductivity at 38 K was reported for $(Ba,K)Fe_2As_2$ first [2].

Indeed, earlier research on P-containing ternary materials with such 122 structure was reported already some time ago (see [3,4] and references therein). After 2008, the field received new momentum when a number of other 122 materials containing either As or P were reported to become superconducting [5–9]. However, the superconducting transition temperature $T_c$ remained rather low with a few kelvins. This fact suggests a possible conventional pairing mechanism in these noniron containing superconductors. In order to substantiate this notion, however, detailed information of the electronic structure is needed here. Especially, accurate knowledge on the degree of two dimensionality is necessary to test for possible nesting between electron and hole bands, essential for the extended $s$-wave pairing scenario as suggested for the iron pnictides [10–14].

A very powerful way for the determination of the Fermi-surface topologies and many-body interactions are measurements of magnetic quantum oscillations. Especially, in combination with state-of-the-art band-structure calculations, this allows the detailed determination of the electronic band structure and of the band-resolved mass enhancement [15,16]. Some recent reviews of such investigations for metallic and superconducting iron pnictides are given in Refs. [17,18].

Here, we report on a detailed de Haas–van Alphen (dHvA) study in combination with band-structure calculations of the 122 iridium phosphide $BaIr_2P_2$. This is a superconductor with a moderate transition temperature of $T_c = 2.1$ K as found for polycrystalline samples [6] and single crystals [7]. Using some of the latter high-quality crystals, we observed dHvA oscillations that agree well with predictions of our band-structure calculations. Besides a strongly corrugated cylindrical, quasi-two-dimensional Fermi-surface sheet, a three-dimensional highly branched Fermi surface is found. Considerable mass-enhancement factors between 1 and 3 are obtained.

The $BaIr_2P_2$ single crystals were grown using a metal-flux technique [19]. In this case, a Pb flux with additional Cu to increase solubility was used. Details of the crystal-growth procedure are given in [7]. Typical sample dimensions used for our experiments are $0.2 \times 0.2 \times 0.02$ mm$^3$. The dHvA effect was measured by use of torque magnetometers. For that CuBe capacitive cantilevers with 25- to 50-$\mu$m thicknesses were fabricated and fixed on platforms that could be rotated *in situ* around one axis. Placing the sample on these cantilevers, the dHvA effect is measured as field-dependent oscillations of the capacitance. The measurements were performed at the Dresden High Magnetic Field Laboratory (HLD) in a superconducting 20-T magnet and at the Grenoble High Magnetic Field Laboratory (LNCMI-Grenoble) using a resistive magnet in fields up to 34 T. In both cases, the cantilevers were mounted directly in the $^3$He/$^4$He mixtures of top-loading dilution refrigerators.

The band structure was calculated using the full-potential local-orbital FPLO code [20]. Exchange and correlation potentials were estimated using the local density approximation [21]. The room-temperature structural data of Ref. [7] were used. We further allowed the P atoms to relax their $z$ position, since we realized that for other 122 compounds this modifies the calculated Fermi surface significantly [16]. In the case of $BaIr_2P_2$ there was a small (0.4%) change in $z$, but the band structure remained unaltered within error bars. Since spin-orbit coupling is relevant for Ir, we also performed full-relativistic calculations. Although this modifies the band

*Current address: Institut für Werkstoffwissenschaft, TU Dresden, D-01062 Dresden, Germany.

 

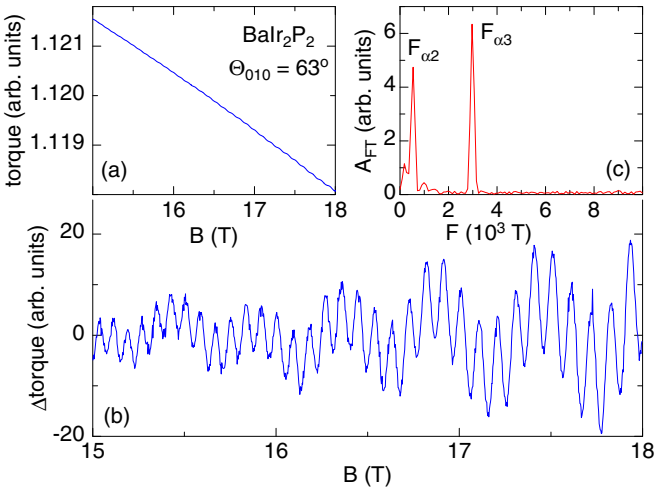


FIG. 1. (Color online) (a) Torque signal of $BaIr_2P_2$ obtained at about 30 mK between 15 and 18 T. The field was rotated by 63° from the $c$ towards the $a$ axis. (b) Oscillating part of the torque signal after background subtraction. (c) Spectrum of the oscillating signal after Fourier transformation with two clearly resolved dHvA frequencies.

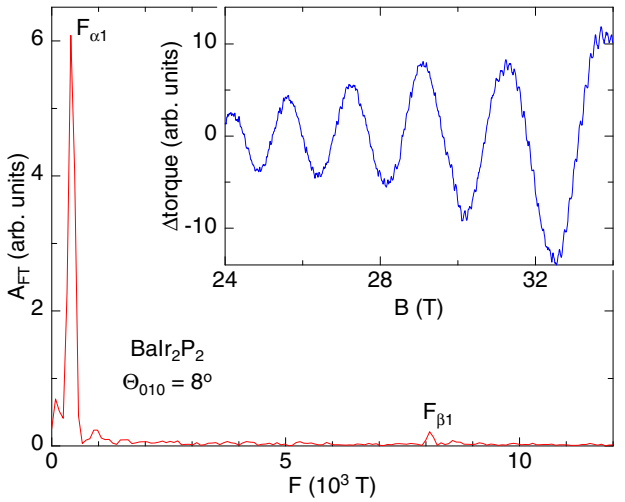


FIG. 2. (Color online) Background-subtracted torque signal (inset) and corresponding Fourier transformation (main panel) measured at about 30 mK at the LNCMI in Grenoble. The field was rotated by 8° from the $c$ towards the $a$ axis.

dispersion far away from the Fermi energy, the Fermi surface, and the effective masses change only marginally [22].

A typical torque signal for our $BaIr_2P_2$ sample is shown in Fig. 1(a). On a smoothly varying background weakly visible oscillations appear. After subtracting the background, using fourth-order polynomials, the oscillating dHvA signal is clearly resolved [Fig. 1(b)], reflecting the excellent signal-to-noise ratio of our torque data. The oscillating data show a fast dHvA oscillation modulated by a slower one. The Fourier transformation confirms the existence of only two fundamental dHvA frequencies at this magnetic-field orientation which are labeled $F_{\alpha 2} = 530$ T and $F_{\alpha 3} = 2975$ T [Fig. 1(c)]. For the shown example, with the magnetic field applied at an angle $\Theta_{010} = 63^\circ$ rotated from the $c$ towards the $a$ axis, the dHvA oscillations have rather large amplitudes with negligible noise. This is not the case for all field orientations. Although we observe dHvA oscillations for all orientations, some dHvA signals appear barely above the noise level.

In order to better resolve such small signals and possibly detect further dHvA branches we performed additional experiments in static fields up to 34 T at the LNCMI in Grenoble. One example of the measured background-subtracted dHvA signal is shown in the inset of Fig. 2. For this field orientation ($\Theta_{010} = 8^\circ$), one strong low dHvA frequency with $F_{\alpha 1} = 429$ T and one weak high frequency ($F_{\beta 1} = 8130$ T) can be resolved. The latter dHvA oscillations are visible at the highest fields in the background-subtracted torque signal and, with a good signal-to-noise ratio, in the Fourier-transformed spectrum (Fig. 2).

We studied the angular dependence of the dHvA oscillations for many different angles by rotating the crystal around the relevant axes of the tetragonal unit cell, namely around the $a$ ($\Theta_{010}$) and $c$ axis ($\Theta_{001}$). The experimentally observed dHvA frequencies are shown in Fig. 3. The data sets measured in Dresden (open symbols) and in Grenoble (closed symbols) agree perfectly. Some of the dHvA branches lead to rather weak amplitudes only and can just be resolved at the highest fields used. As a measure of the relative dHvA amplitudes we converted the logarithm of these amplitudes to symbol sizes in Fig. 3 [23]. In other words, the small symbols of, e.g., the branches $\alpha_4$ and $\beta_1$ depict the fact that the corresponding dHvA amplitudes are 10–20 times smaller than, e.g., some of the $\alpha_1$ amplitudes.

The solid lines in Fig. 3 show the angular dependence of the extremal orbits as obtained from band-structure calculations. For that, the FPLO code was used resulting in the dispersion relations as shown in Fig. 4. There are two bands crossing the Fermi energy, colored in green (band 49) and red (band 50). The main contributions to band 49 (50) arise from 31% (34%) Ir $5d$, 21% (10%) Ba $5d$, and 28% (39%) P $3p$ orbitals.

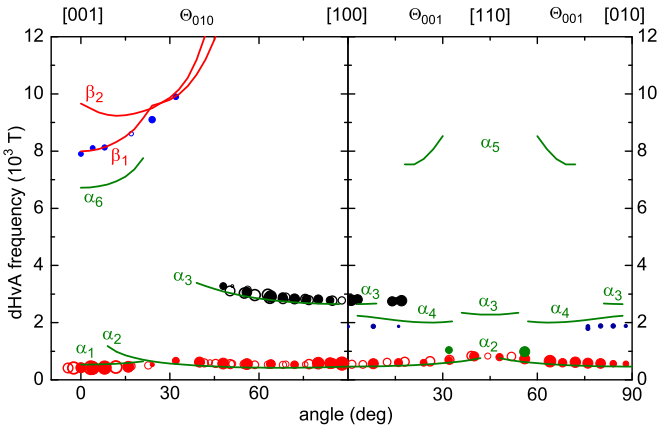


FIG. 3. (Color online) Angular dependence of the measured (symbols) and calculated (lines) dHvA frequencies. The open symbols were obtained at the HLD in Dresden in magnetic fields up to 18 T and the closed symbols at the LNCMI in Grenoble in fields up to 34 T. The symbol size is a measure of the Fourier-transformation amplitude [23].

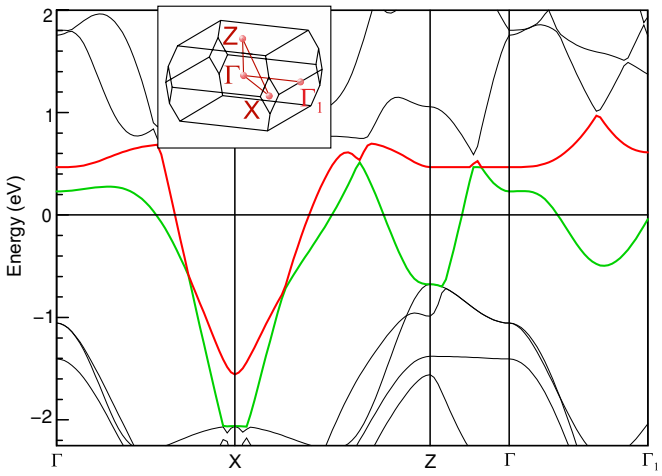


FIG. 4. (Color online) Band structure of $BaIr_2P_2$ calculated using the FPLO code. Two bands, colored in red and green, are crossing the Fermi energy, set to zero. The inset shows the Brillouin zone with symmetry points.

Having such dispersion relations calculated for a dense $24 \times 24 \times 24\,k$ mesh, we obtain the Fermi surfaces of the two bands as shown in Fig. 5. Thereby, the red-colored band in Fig. 4 leads to a strongly corrugated quasi-two-dimensional cylindrical Fermi surface [Fig. 5(a)], whereas the multiconnected complicated Fermi surface in Fig. 5(b) originates from the green-colored band in Fig. 4. Some of the extremal cross sections, i.e., of the orbits leading to dHvA oscillations, for fields aligned along $c$ and roughly along $a$ are shown by solid lines in Fig. 5 [24].

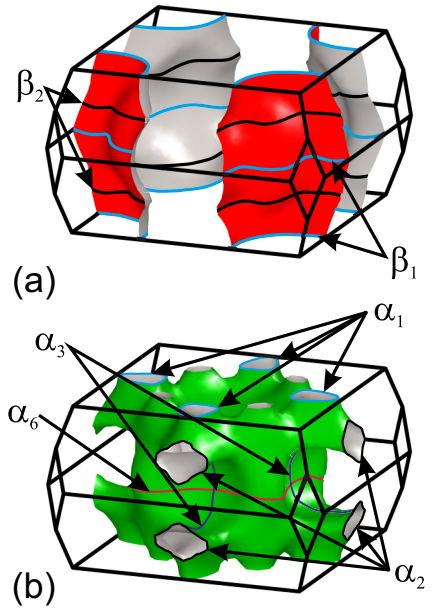


FIG. 5. (Color online) Calculated Fermi surface of $BaIr_2P_2$ originating from (a) the red and (b) green band crossing the Fermi energy (Fig. 4). Some of the dHvA orbits are depicted by solid lines and labeled.

TABLE I. Comparison between calculated and measured dHvA frequencies and effective masses for different bands and field orientations in $BaIr_2P_2$.

| | | Measured | | Calculated | |
|---|---|---|---|---|---|
| $\Theta_{010}$ | orbit | $F$ (T) | $m/m_e$ | $F$ (T) | $m_b/m_e$ |
| 8° | $\alpha_1$ | 429 | 1.0(3) | 545 | 0.27 |
| 8° | $\beta_1$ | 8130 | – | 8135 | 0.74 |
| 55° | $\alpha_2$ | 540 | 1.0(4) | 436 | 0.38 |
| 55° | $\alpha_3$ | 3030 | 1.3(1) | 2930 | 0.64 |

A comparison between the calculated and measured dHvA frequencies for some orbits is given in Table I. The agreement between theory and experiment is excellent, especially when taking into account that no adjustable parameter was used. This very good agreement can as well be seen in Fig. 3 where the calculated dHvA frequencies (lines) coincide nicely with measured data. Only for some angles theory predicts a few additional dHvA orbits that are not seen in experiment, maybe due to their small dHvA amplitudes. Indeed, the calculated band masses of these latter orbits lie between about 1 and 2.1 $m_e$, i.e., are considerably larger than calculated for the experimentally observed orbits (see below). Together with a Dingle temperature of about 4.7 K, as obtained for the $\alpha_3$ orbit, much weaker dHvA signals than the ones observed are expected for these heavier-mass orbits; i.e., these predicted dHvA orbits might have signal amplitudes that most probably are below our resolution limit. On the other hand, the experimentally observed dHvA signals, such as the $\beta_1$ frequencies, fit perfectly to the predicted data, even in absolute numbers, and the angular dependences of all observed $\alpha$ frequencies are well reproduced. In absolute numbers, the difference for the latter frequencies seems large at first sight. However, taking into account that the cross section of the total Brillouin zone perpendicular to $c$ is about 33 kT, the difference between the calculated and measured values is only about 0.4% of that area.

For selected angles, we determined the effective masses $m$ of some dHvA orbits from the temperature dependence of the dHvA amplitudes [25,26]. The extracted values, summarized in Table I, are close to the free-electron mass $m_e$ [27]. The dHvA amplitude of the $\beta_1$ orbit could not be determined reliably over a large-enough temperature range preventing a reasonable extraction of $m$ here. Although the measured effective masses are rather small, they are still 2–4 times larger then the band masses $m_b$, obtained from our band-structure calculations (Table I). Additionally, the Sommerfeld coefficient $\gamma = 9.3$ mJ/molK$^2$ as estimated in Ref. [7] is enhanced by a factor of 18 compared to the calculated 0.53 mJ/molK$^2$. Obviously, strong many-body interactions exist in $BaIr_2P_2$ leading to equivalent mass-enhancement factors, $\lambda = m/m_b - 1$, between 1 and 3 for the $\alpha$ orbits. Indeed, the corresponding (green) band [Fig. 5(b)] contributes about 76% to the total density of states at the Fermi level. Consequently, if $\lambda$ is mainly caused by electron-phonon interactions, $BaIr_2P_2$ would be a strong-coupling superconductor with, however, only a moderate $T_c$ of 2.1 K.

Somewhat smaller, but still considerable mass enhancements have been found for another non-iron-containing 122 superconductor, namely $BaNi_2P_2$ with $T_c = 2.51$ K [28]. Although not explicitly, the authors of that work suggest a phonon-mediated mechanism for superconductivity, based on a theory work proposing such Cooper-pair coupling for the isostructural material $BaNi_2As_2$ [29]. It seems plausible to expect such coupling as well in the present superconductor. Indeed, for all above-mentioned materials the Fermi-surface topology is largely different from the pronounced two-dimensional electronic structure of the superconducting 122 iron pnictides. Therefore, extended $s$-wave pairing, as suggested for the latter materials [10–14], can be ruled out as the mechanism responsible for superconductivity in $BaIr_2P_2$ since the essential nesting condition is missing.

In conclusion, our angular-dependent dHvA data are in excellent agreement with predictions from band-structure calculations giving us a detailed picture of the Fermi-surface topology of $BaIr_2P_2$. Only two bands are crossing the Fermi energy and the resulting Fermi surface is highly three-dimensional, contrary to iron-containing 122 superconductors. We observe rather strong enhancements in the measured effective masses. Although this points to strongly coupled Cooper pairs, the superconducting transition temperature is rather low. More detailed calculations taking into account the phonon dynamics and density of states would be necessary to verify the suggestion of such an electron-phonon coupling scenario.

The research at UdeM received support from the Natural Sciences and Engineering Research Council of Canada (Canada), Fonds Québécois de la Recherche sur la Nature et les Technologies (Québec), and the Canada Research Chair Foundation. We acknowledge support from HLD at HZDR and LNCMI, members of the European Magnetic Field Laboratory (EMFL), and the Deutsche Forschungsgemeinschaft (SPP 1458).

[1] Y. Kamihara, T. Watanabe, M. Hirano, and H. Hosono, J. Am. Chem. Soc. **130**, 3296 (2008).
[2] M. Rotter, M. Tegel, and D. Johrendt, Phys. Rev. Lett. **101**, 107006 (2008).
[3] W. Jeitschko and M. Reehuis, J. Phys. Chem. Solids **48**, 667 (1987).
[4] W. Jeitschko, R. Glaum, and L. Boonk, J. Solid State Chem. **69**, 93 (1987).
[5] T. Mine, H. Yanagi, T. Kamiya, Y. Kamihara, M. Hirano, and H. Hosono, Solid State Commun. **147**, 111 (2008).
[6] D. Hirai, T. Takayama, R. Higashinaka, H. Aruga-Katori, and H. Takagi, J. Phys. Soc. Jpn. **78**, 023706 (2009).
[7] N. Berry, C. Capan, G. Seyfarth, A. D. Bianchi, J. Ziller, and Z. Fisk, Phys. Rev. B **79**, 180502(R) (2009).
[8] F. Ronning, E. D. Bauer, T. Park, S.-H. Baek, H. Sakai, and J. D. Thompson, Phys. Rev. B **79**, 134507 (2009).
[9] K. Kudo, Y. Nishikubo, and M. Nohara, J. Phys. Soc. Jpn. **79**, 123710 (2010).
[10] I. I. Mazin, D. J. Singh, M. D. Johannes, and M. H. Du, Phys. Rev. Lett. **101**, 057003 (2008).
[11] M. M. Korshunov and I. Eremin, Phys. Rev. B **78**, 140509(R) (2008).
[12] V. Cvetkovic and Z. Tesanovic, Europhys. Lett. **85**, 37002 (2009).
[13] I. I. Mazin, Nature (London) **464**, 183 (2010).
[14] K. Kuroki, S. Onari, R. Arita, H. Usui, Y. Tanaka, H. Kontani, and H. Aoki, Phys. Rev. Lett. **101**, 087004 (2008).
[15] B. Bergk, V. Petzold, H. Rosner, S.-L. Drechsler, M. Bartkowiak, O. Ignatchik, A. D. Bianchi, I. Sheikin, P. C. Canfield, and J. Wosnitza, Phys. Rev. Lett. **100**, 257004 (2008).
[16] S. Blackburn, B. Prévost, M. Bartkowiak, O. Ignatchik, A. Polyakov, T. Förster, M. Côté, G. Seyfarth, C. Capan, Z. Fisk, R. G. Goodrich, I. Sheikin, H. Rosner, A. D. Bianchi, and J. Wosnitza, Phys. Rev. B **89**, 220505(R) (2014).
[17] A. Carrington, Rep. Prog. Phys. **74**, 124507 (2011).
[18] A. I. Coldea, D. Braithwaite, and A. Carrington, C. R. Physique **14**, 94 (2013).
[19] P. C. Canfield and Z. Fisk, Philos. Mag. B **65**, 1117 (1992).
[20] K. Koepernik and H. Eschrig, Phys. Rev. B **59**, 1743 (1999).
[21] J. P. Perdew and Y. Wang, Phys. Rev. B **45**, 13244 (1992).
[22] We performed spin-polarized calculations with an initial polarization, but they quickly converge towards a zero magnetization. Additionally, fixed-spin-moment calculations show no local or global minima, besides zero magnetization.
[23] Scaling between the low-field (HLD) and high-field (LNCMI) data was done by just one factor.
[24] The orbits $\alpha_4$ and $\alpha_5$ lie in the interior of the shown Fermi-surface sheet [Fig. 5(b)] and cannot be visualized in this plot.
[25] I. M. Lifshitz and A. M. Kosevich, Zh. Eksp. Teor. Fiz. **29**, 730 (1955) [Sov. Phys. JETP **2**, 636 (1956)].
[26] D. Shoenberg, *Magnetic Oscillations in Metals* (Cambridge University Press, Cambridge, 1984).
[27] The relatively large error bars of the effective masses are caused by the restricted temperature range accessible in the dilution refrigerators. At the highest temperatures of about 1 K, the dHvA amplitudes are reduced only slightly leading to large uncertainties in $m$.
[28] T. Terashima, M. Kimata, H. Satsukawa, A. Harada, K. Hazama, M. Imai, S. Uji, H. Kito, A. Iyo, H. Eisaki, and H. Harima, J. Phys. Soc. Jpn. **78**, 033706 (2009).
[29] A. Subedi and D. J. Singh, Phys. Rev. B **78**, 132511 (2008).